9th International Workshop on Simulation for Energy, Sustainable Development & Environment
18th International Multidisciplinary Modeling & Simulation Multiconference

ISSN 2724-0061 ISBN 978-88-85741-67-6 © 2021 The Authors.
doi: 10.46354/i3m.2021.sesde.005

Mathematical and numerical investigations of diffusion in silicon based solar cells

El Boukili Abderrazzak [1,*]

[1]Al Akhawayn University, P.O. Box 104 Avenue Hassan II, Ifrane, 53000, Morocco

[*]Corresponding author. Email address: a.elboukili@aui.ma

Abstract
The goal of this paper is to develop and apply an accurate mathematical model to investigate and optimize the effects of texturing on the diffusion of dopants in modern textured solar cells. This investigation will help out the manufacturers and designers of solar cells optimize the texturing geometry and its parameters. The findings in this paper will also help maximize the optical and electrical performance of innovative solar cells and reduce their production cost. For example, non-optimized texturing pyramids obtained from a texturing chemical reaction will reduce the absorption of the sun light. It will also cause excessive defects on the surface of the cell which will affect negatively the diffusion of dopants and the solar cell efficiency. We found that texturing angles around 30° could improve both the diffusion of dopants and the efficiency of the solar cell. Two dimensional numerical results showing the effects of texturing geometry on boron ion diffusion in a sample solar cell will be presented, analyzed, and validated with literature.

Keywords: New models; simulation; texturing geometry; diffusion; solar cells

1. Introduction

The main objective of this paper is to develop and apply an accurate mathematical model to study and optimize the effects of texturing geometry on dopants' diffusion in innovative silicon based solar cells. Ion diffusion process is used, after ion implantation process, in the fabrication of modern solar cells to activate of the implanted ions, reduce the implantation defects, and improve the passivation of the front and rear surfaces.

In our previous paper (El Boukili 2019), we have studied the effects of texturing angles on ion implantation. In this paper, we are studying the effects of texturing angles on ion diffusion.

In recent years, solar energy market has experienced an exponential growth thanks to the government policies throughout the world. However, the cost of electricity coming from the solar cells is still higher that of grid electricity. Therefore, many innovative techniques have been used in the fabrication of recent solar cells to reduce cost and increase efficiency.

Ion implantation and ion diffusion is among the techniques of choice for the fabrication of the modern silicon based and high efficient solar cells (Bothe, 2005); (Ohrdese at al, 2011); (Zimbardi et al, 2012);(Rohatgi et al, 2012); (Pawlak et al, 2012); (Benick et al, 2009); (Ohrdes et al, 2011); (Zimbardi et al, 2012); (Coletti et al, 2012); (Meier et al, 2010).

Ion implantation and ion diffusion processes have many advantages over the blanket doping and diffusion processes. Ion implantation and ion diffusion allow better control of the doping doses, doping depths, doping profiles, doping-induced defects, diffusion profiles, and activation of the dopants and defects.

© 2021 The Authors. This article is an open access article distributed under the terms and conditions of the Creative Commons Attribution (CC BY-NC-ND) license (https://creativecommons.org/licenses/by-nc-nd/4.0/).

Texturing is another innovative technique in recent photovoltaic industry to enhance the optical absorption of crystalline silicon solar cells and make lower cost solar cells. Optimized texturing geometry and texturing parameters could reduce the sun light reflection losses at the top and bottom surfaces of solar cells by more than 10% (Netsor et al, 2010).

After the texturing processes, the top and bottom surfaces will consist of square pyramids of different heights, lengths, widths, and angles. Obtaining pyramids with optimal geometry is still a challenge. One of the goals of this paper is to investigate the effects of the geometry of these pyramids on the ion diffusion profiles to help predict the optimal geometry of texturing and get high efficient and low cost solar cells.

We should note that ion implantation and ion diffusion in textured solar cells is significantly different from ion implantation and ion diffusion in planar solar cells.

Specially, texturing will increase the surface area of the solar cell and introduce extra defects. These extra defects will impact the activation of the dopants during the diffusion process. They will also make it difficult to predict the diffusion parameters as: temperature, pressure, time and so on. On the other hand, the increase of the surface area will lead to a reduction in the effective dose of the implanted ions. This reduction of the effective dose depends mainly on the geometry of the pyramids obtained from texturing process and the texturing angle θ. We define the texturing angle θ as the angle between the incident ions and the normal

n to a given face of a pyramid on the surface of the solar cell. Each pyramid has four faces. We are taking an arbitrary face.

The originality of this paper is the development and application of an accurate mathematical model to study, analyze, and optimize the impact of texturing angles θ on the ion diffusion in textured solar cells under different temperatures, and diffusion times.

This paper is organized as follows. Section 2 presents the diffusion models we have developed to include the effects of θ on ion diffusion. Section 3 presents the numerical results for ion diffusion profiles with different texturing angles, temperatures and diffusion times. This section will also present a qualitative comparison between the obtained results and experimental results found in literature.

Section 4 summarizes the concluding thoughts and future work.

2. Mathematical models for ion diffusion in textured solar cells

The efficiency of a solar cell depends on the fabrications processes such as texturing of the surfaces of the cell. Texturing increases the surface absorption area of the incident radiation on the cell. Consequently, it reduces the substrate reflectance and increases efficiency of the cell, see Figure 1.

However, ion implantation and ion diffusion is more challenging in solar cells with textured surfaces than in solar cells with flat surfaces. To help designers and manufacturers understand and optimize the effects of texturing geometry on ion diffusion, we are developing here a comprehensive set of ion diffusion models that take into account the effects of texturing angle θ on ion diffusion in textured solar cells.

The thermal diffusion is needed to activate the implanted (or dopant) ions (A) and to repair the damage caused by the implantation process. The implantation damage is represented by the existence of the point-defects. The point-defects are represented by interstitial ions (I) and vacancy ions (V). The thermal diffusion of all these charged ions A, I, and V is due to their unequal concentrations and to the internal electric field.

The derivation of the coupled diffusion equations for the ions A, I, and V is based on the continuum theory using Fick's laws and the atomistic theory. The advanced models of ion diffusion are based on the idea of pair-diffusion. This means, most of the impurity atoms, A, can't diffuse on their own. But, they need the neighboring point-defects I and V as diffusion vehicles as shown if Figure 3.

When a binding energy between an impurity A and a neighboring defect I or V is not weak, the impurity A and the point defect I or V will move as a pair impurity-defect AI or AV until they get separated by a recombination or other factors. There are mainly three different diffusion mechanisms:

1. Direct diffusion mechanism

Here, impurities A which have small ionic radii can travel from one interstitial site to another. For example, group I and III elements are diffusing directly and they are fast diffusers.

2. Vacancy mechanism

A substitutional dopant exchanges its position with an adjacent or a neighboring vacancy. The vacancy should move at least to the third neighbor site away from a dopant to avoid oscillations.

3. Interstitial mechanism

In Silicon material, the dopant at a substitutional site is approached by a Silicon interstitial and kicked out to live at an interstitial location. The original self-interstitial move to reside in a regular lattice location.

We should note that a dopant (A) can diffuse only when it is paired with I or V. Then, the dopants have paired diffusion. Some dopants will diffuse with vacancies only, some with interstitials only and some could diffuse with both. For example, Boron will diffuse with interstitials. Phosphorus will diffuse with

interstitials at low doping and with interstitials and vacancies at high doping.

However, the defects I or V can move freely alone (unpaired diffusion) or move in a pair with a dopant A (paired diffusion). The diffusivity coefficients of paired and unpaired defects could be very different. The diffusion equations of free defects I or V will be different than the diffusion equations of the paired defects. The diffusion equations of free defects will be given explicitly. The diffusion equations of paired defects are similar to those of paired dopants.

Let $C_T(x,t)$ be the total concentration of all the ionized dopants after t seconds of thermal diffusion. Let $C_{TI}(x,t)$, and $C_{TV}(x,t)$ be the total concentrations of interstitials and vacancies . We have:

$$C_T(x,t) = C_A(x,t) + C_{AI}(x,t) + C_{AV}(x,t) \quad (1)$$

$$C_{TI}(x,t) = C_I(x,t) + C_{AI}(x,t) \quad (2)$$

$$C_{TV}(x,t) = C_V(x,t) + C_{AV}(x,t) \quad (3)$$

Where $C_A(x,t)$, $C_I(x,t)$, and $C_V(x,t)$ are the concentrations of the unpaired dopants, interstitials and vacancies, respectively. The $C_{AI}(x,t)$, and $C_{AV}(x,t)$ are the concentrations of the paired dopants (A) or the paired interstitials (I) or vacancies (V).

At intrinsic doping concentrations ($C_T \leq n_i$), the diffusion flux J_T of each dopant C_T due to the gradient of the concentration C_T is modelled by the Fick's first law as follows:

$$J_T = D_T.\nabla C_T \quad (4)$$

Where D_T is the diffusion coefficient, and n_i is the intrinsic electron concentration. At diffusion temperatures, the dopant ions are usually ionized, and the released electrons cause an electric field E and an electrostatic potential φ that will affect the diffusion flux. The diffusion flux J_T will include a field enhancement term (drift term) as follows:

$$J_T = D_T.\nabla C_T + v.C_T \quad (5)$$

The velocity v of the charged particles can be described with:

$$v = \mu E = -\mu \nabla \varphi \quad (6)$$

The mobility μ is related to the diffusion coefficient by Einstein's relation:

$$v = D_T . \frac{q}{kT} \quad (7)$$

Where q is the elementary charge, k is the Boltzmann constant, and T is the temperature. By including the equations (6) and (7) in (5), the Fick's first law is extended to:

$$J_T = -D_T(\nabla C_T + z_T \frac{q}{kT} C_T \nabla \varphi) \quad (8)$$

Where z_T denotes the charge states of the dopant ions. For singly charged acceptors z_T = -1. For singly charged donors z_T =+1.

From Equation (8), we should note that the flux J_T of a given diffusing species $C_T(x,t)$ will be coupled to all the other ionized dopants. Let $C_i(x)$ be the concentration of the dopant number 'i' obtained after a doping process. This coupling is introduced by the presence of the electrostatic potential φ which depends on all the ionized dopants through Poisson's Equation as follows:

$$div(\varepsilon \nabla \varphi) = q.(n - p - C_{net}) \quad (9)$$

Where

$$C_{net} = -\sum_{i=1}^{N} z_i C_i(x) \quad (10)$$

Here n, and p are the concentrations of the free electrons and holes, respectively. By assuming thermal equilibrium, Boltzmann statistics, and charge neutrality, we get:

$$\varphi = \frac{kT}{q} . \ln((\frac{C_{net}}{2n_i})^2 + \sqrt{(\frac{C_{net}}{2n_i})^2 + 1}) \quad (11)$$

$$n = n_i \exp(\varphi \frac{q}{kT}) \quad (12)$$

$$p = n_i \exp(-\varphi \frac{q}{kT}) \quad (13)$$

From Eq. (12), we get:

$$\frac{q}{kT} \nabla \varphi = \nabla \ln(\frac{n}{n_i}) \quad (14)$$

Then, the flux J_T of each diffusing ion (I, V, AI, AV, or other) will be given for each n-type by:

$$J_T = -D_T(\nabla C_T + C_T \nabla \ln(\frac{n}{n_i})) \quad (15)$$

For p-type ions as Boron, n is replaced by p. In Eq. (11), we are ignoring the charge states of the diffusing ions. We have:

$$\nabla C_T + C_T \nabla \ln(\frac{n}{n_i}) = C_T \nabla \ln(C_T \frac{n}{n_i}) \quad (16)$$

Then, we get the final form of the flux equation of each 5 species A, I, V, AI, AV:

$$J_f = D_f C_f \nabla \ln(C_f \frac{n}{n_i}) \quad (17)$$

Here, $f = A, I, V, AI$ or $f = AV$. Using the Fick's second law, we get the continuity equation of each 5 species A, I, V, AI, AV:

$$\frac{\partial C_f(x,t)}{\partial t} = div(J_f) - R_f \quad (18)$$

Where, R_f represents all the possible sources of the net recombination or generation rates between different ions A, I, V, AI, AV (scup). A simple expression for R_f is given by:

$$R_f = K_f(C_I C_V - C_I^* C_V^*) \quad (19)$$

Where, K_f is a constant and C_I^*, C_V^* are the concentrations of the free ions I, V at equilibrium.
As found in literature, the unpaired dopants, A, are assumed to be immobile. Then, their flux J_A is null. Finally, the 5 equations of the model describing the coupled diffusion of a single n-type dopant with point-defects I and V are given by:

$$\frac{\partial C_A(x,t)}{\partial t} = R_A \quad (20)$$

$$\frac{\partial C_{AI}(x,t)}{\partial t} = -div(J_{AI}) + R_{AI} \quad (21)$$

$$\frac{\partial C_{AV}(x,t)}{\partial t} = -div(J_{AV}) + R_{AV} \quad (22)$$

$$\frac{\partial C_I(x,t)}{\partial t} = -div(J_I) + R_I \quad (23)$$

$$\frac{\partial C_V(x,t)}{\partial t} = -div(J_V) + R_V \quad (24)$$

To introduce the effects of the texturing angles θ on all these coupling diffusion Equations 20-24, we define the dopant concentration $C_i(x)$ in Eq. 10 by:

$$C_i(x) = C_i(x,\theta) \quad (25)$$

Then, we use Gauss probability function to estimate $C_i(x,\theta)$ as follows:

$$C_i(x,\theta) = \frac{\phi\cos(\theta)}{\sqrt{2\pi\sigma}} \exp\left[-\frac{(x-R)^2}{2\sigma}\right] \quad (26)$$

The parameters in Eq. 26 are described in our previous work (El Boukili, 2019). Pearson IV probability function could be used as well in Eq. 26.

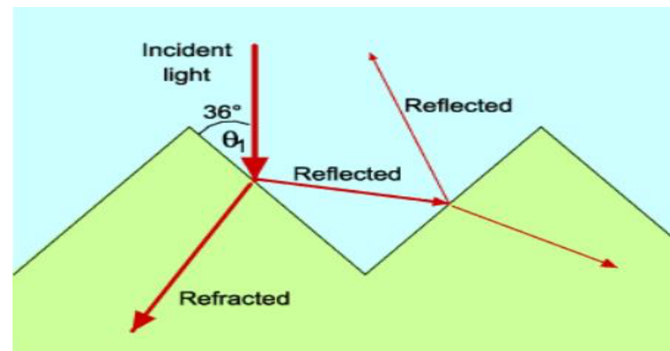

Figure 1. Sun light absorbed by pyramids

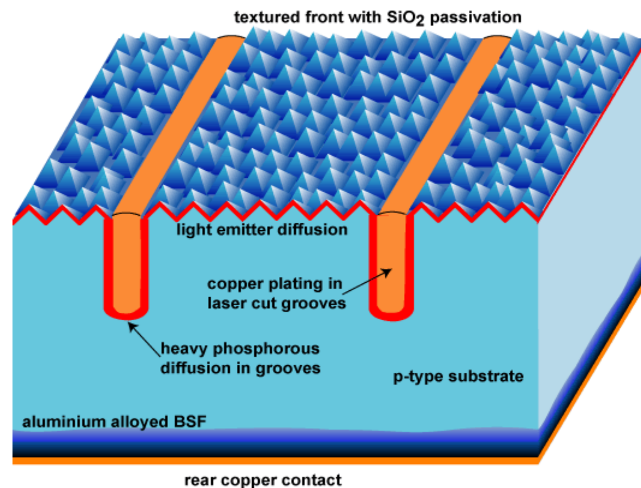

Figure 2. Textured solar cell with random pyramids

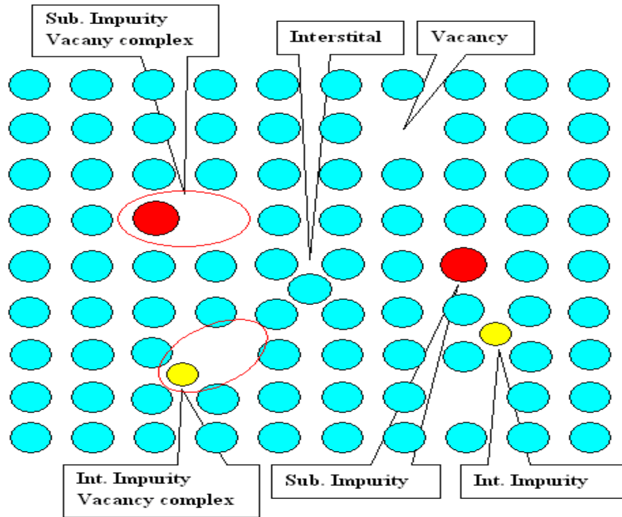

Figure 3. Atomic structure after ion implantation

3. Numerical results and validation

We use an N-type silicon (001) solar cell textured with identical pyramids of faces (111) as shown in Figure 2. The texturing angle α was varied from 20° to 64° degrees. The height of pyramids is 0.12um. The width of the pyramids is 0.05um. The dose of Boron is $2\times10^{15}cm^{-2}$, implant energy is 10 KeV, the implant model is $fn(y,\alpha)$. The depth, y, of the cell is 0.37 um and the length, x, is 0.3 um.

Figure 4 shows the Boron diffusion profileon textured solar cell for α =36°. Figure 5 shows the 1D cut of the Boron diffusion profile at x=0.15 and α =36° and y between 0 um and 0.15 um. Figure 4 shows the cut of the Boron doping profile at x=0.15 and α =64° and y between 0 um and 0.15 um. Figure 6 shows the cut of the Boron diffusion profile at x=0.15 and y between 0 um and 0.15 um when the surface of the solar cell is not textured. By comparing Figure 6 with Figures 5 and 4, we see that the texturing of the solar cell changes significantly the diffusion profile. This will affect significantly the efficiency of the textured solar cell.

From the Figures 5 and 6, two effects are visible: (i) reduction of the Boron distribution values with increasing α. (ii) reduction of the diffusion depth with increasing α. The first effect could be explained by the reduction of the effective dose due to the angle α as shown by the Equation (1). The other effect (ii) could also be explained by the reduction of the effective dose due to the angle α. Small ion doses will produce shallow diffusion profiles seen in ii). For α =36°, the maximum value of the diffused Boron is 1.2e+20 (atom/cm-2) (see Figure 5). For α =64°, the maximum value of the diffusion Boron is 7e+19 (atom/cm-2) (see Figure 6). These 2 values are smaller than the maximum value of the diffused Boron on non-textured surface which is 4e+20 (atom/cm-2) (see Figure 7). The diffusion depth on textured surface for α =36° is about 0.06 um and on non-textured surface for α =0° is about 0.08 um. From these simulation results, we could suggest to use smaller texturing angles α around 30° for ion implantation on textured surfaces if shallow profiles are not needed. On the other hand, it has been shown in (Zahi, 2018), that with smaller angles α around 36°, the measurements of doping profiles in textured solar cells using the secondary ion mass spectrometry (SIMS) technique are more accurate than with larger angles. We should note that the measurements of doping and diffusion profiles using SIMS technique are strongly depending on the texturing angles α as well. The Boron diffusion profiles obtained in this simulation are in a good agreement with SIMS measured profiles obtained in (Zahi et al, 2018).

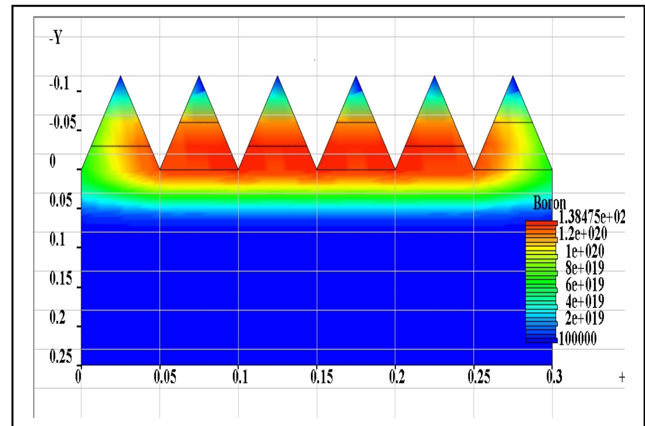

Figure 4. 2D Boron diffusion profile on textured solar cell for α =36°

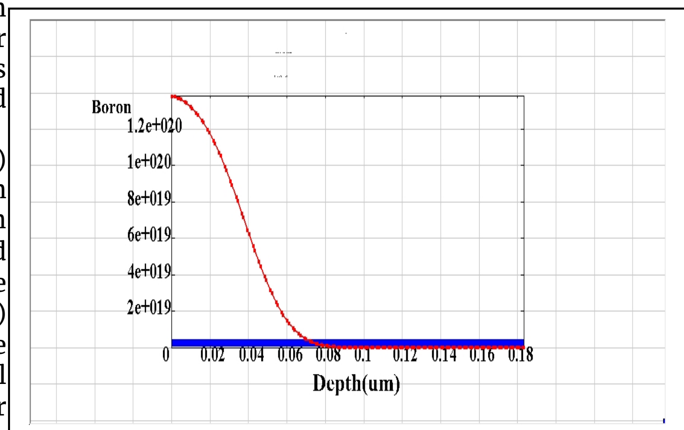

Figure 5. 1D Cut of Boron diffused profile on textured surface for α =36°

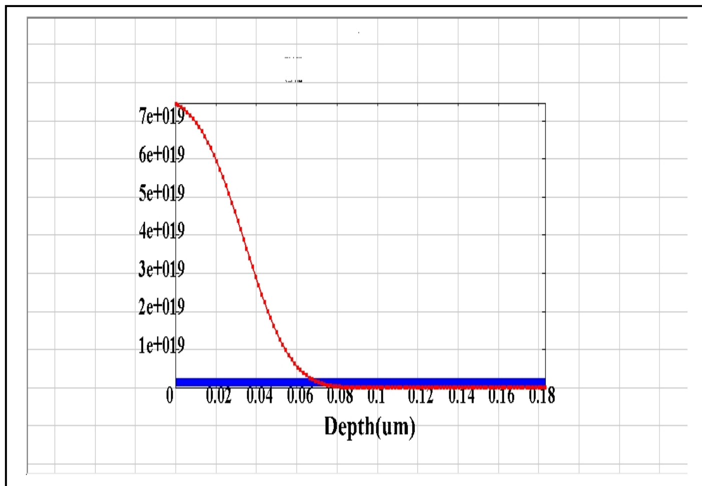

Figure 6. Boron diffused profile on textured surface for α =64°

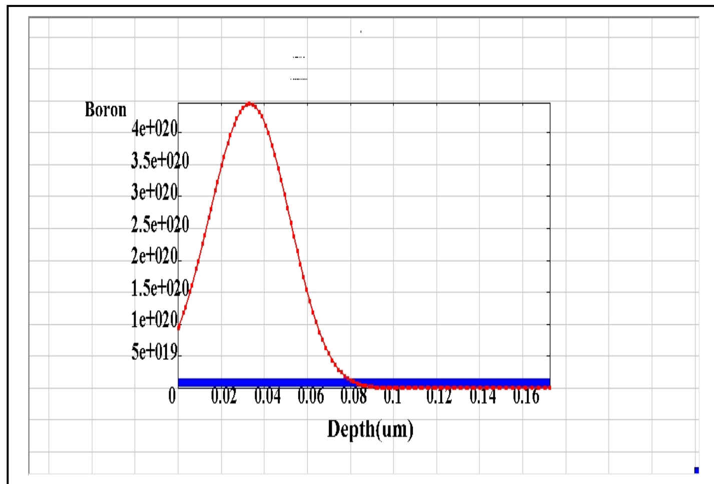

Figure 7. Boron diffused profile on non-textured surface for α =0°

4. Conclusions

We have shown that the texturing angle α affects significantly the doping profiles in textured solar cells. The values of the doping and the implantation depth are decreasing with increasing α. By comparing the doping profiles on planar surface shown in Figure 5 with doping profiles on textured surfaces shown in Figures 3 and 4, we see that the shape of the doping profiles are also affected by the texturing angle α. In future work, we will investigate the effects of the size of the pyramids on the doping profiles.

References

Bothe, K., Sinton, R., and Schmidt, J. (2005). Fundamental boron-oxygen-related carrier lifetime limit in mono- and multicrystalline silicon. Progress in Photovoltaics Research and Applications 13(4):287 – 296.

Ho, W., Huang, Y., Hsu, W., Chen, Y., and Liu, C. (2011). Ion implanted boron emitter N-silicon solar cells with wet oxide passivation. 37th IEEE Photovoltaic Specialists Conference, Seattle, WDC, USA.

Fabian, K., Tobias, O., Robby, P., and Rolf, B. (2011). Analyzing the recombination current densities in industrial like n-type PERT solar cells exceeding 20% efficiency. 23rd IEEE Photovoltaic Specialists Conference, Seattle, WDC, USA.

Kveder, V., Kittler, M., and Schroter, W. (200)1. Recombination activity of contaminated dislocations in silicon: A model describing electron-beam-induced contrast behavior. Physics Review, B, 63:115208.

Benick, J., Hoew, B., Van, M., Kessels, O., Schultz, O., and Glunz, W. (2008). High efficiency n-type si solar cells on alo-passivated boron emitters. Applied Physics Letters, Vol., 92:253504.

Benick, J., Hoew, B., Dingemans, G., Richter, A., Hermle, M., and Glunz, W. (2009). High efficiency n-type si solar cells with front side boron emitter. Proceedings of the 24th European Photovoltaic Solar Energy Conference, 863-870.

Ohrdes, T., Steingrube, S., Wagner, H., Zechner, C., Letay, G., Chen, R., Dunham, S., and Altermatt, P. (2011). Solar cell emitter design with pv-tailored implantation. Energy Procedia, Vol., 8:167-173.

Zimbardi, F., Upadhyaya, D., Tao, Y., OK, Y., Ning, S., and Rohatgi, A. (2012). Ion implanted and screen-printed large area 19.6% efficiency n-type bifacial si solar cell. Photovoltaic Specialits Conference, 002240-002243.

Rohatgi, A., Meier, B., McPherson, B., OK, Y., Upadhyaya, D., Lai, H., and Zimbardi, F. (2012). High-throughput ion-implantation for low-cost high efficiency silicon solar cells. Energy Procedia, Vol., 15:10-19.

Glunz, S., Rein, S., Lee, J., and Warta, W. (2001). Minority carrier lifetime degradation in boron doped czochralski silicon. Journal of Applied Physics, Vol., 90, 5:2397-2404.

Geerligs, L. and Machdonald, L. (2004). Recombination activity of interstitial iron and other transition metal point defects in p-type crystalline silicon. Applied Physics Letters, Vol., 85, 18:4061-4063.

Coletti, G., Mihailetchi, V., Komatsu, Y., Geerligs, L., Kvande, R., Arnberg, L. Wambach, K., Knopf, C., Kopecek, R. and Weeber, A. (2012). Large area screen printed n-type base silicon solar cells with efficiency exceeding 18%. Solar energy, Vol., 2011:2010.

Pawlak, B., Janssens, T., Singh, S., Kuzma, I., Robbelei, J., Posthuma, N., Poortmans, J., Cristioan, F. and Bazizi, E. (2012). Studies of implanted boron emitters for solar cell applications. Progress in Photovoltaic: Research and Applications, Vol. 20, no. 1:106-110.

Benick, J., Hoex, B., Dingemans, G., Richter, A., Hermle, M. and Glunz, S. (2009). High efficiency n-type silicon solar cells with front side boron emitter. Proceedings of the 24th European Photovoltaic Solar nergy Conference, 863-870.

Meier, D. and Rohatgi, A. (2010). Developing novel low-cost, high-throughput processing techniques for 20% efficient monocrystalline silicon solar cells. Photovoltaics Internation, Vol. 10:87-93.

Bateman, N., Sullivan, P., Reichel, C., Benick, J., Hermle, D., and Rohatgi, D., A. (2011). High quality ion implanted boron emitters in an inter-digitated back contact solar cell with 20% efficiency. Energy Procedia, Vol., 8:509-514.

Ryu, K., Upadhyaya, A., Ok, W., Xu, H., Metin, L., and Rohatgi, N. (2012). High efficiency n-type solar cells with screen-printed boron emitters and ion-implanted back surface field. Photovoltaic Specialists Conference, 38th IEEE, 002247-002249.

El Boukili, A. (2019). Modeling and analysis of the impact of texturing angles on doping profiles in ion implanted N-type solar cells. Proceedings of the 7th International Workshop on Simulation for Energy, Sustainable Development & Environment (SESDE 2019), 1-6. DOI: https://doi.org/10.46354/i3m.2019.sesde.001.